MNRAS **000**, 1–8 (2015) Preprint 6 May 2016 Compiled using MNRAS LATEX style file v3.0

On the temperature dependence of the rate coefficient of formation of C_2^+ from C + CH^+

S. Rampino,[1]★ M. Pastore,[2] E. Garcia,[3] L. Pacifici[4] and A. Laganà[4]
[1]*Istituto di Scienze e Tecnologie Molecolari, Consiglio Nazionale delle Ricerche, c/o Dipartimento di Chimica, Biologia e Biotecnologie, Università degli Studi di Perugia, Via Elce di Sotto 8, Perugia 06123, Italia*
[2]*Computational Laboratory for Hybrid and Organic Photovoltaics (CLHYO), Istituto di Scienze e Tecnologie Molecolari, Consiglio Nazionale delle Ricerche, c/o Dipartimento di Chimica, Biologia e Biotecnologie, Università degli Studi di Perugia, Via Elce di Sotto 8, Perugia 06123, Italia*
[3]*Departamento de Química Física, Universidad del País Vasco (UPV/EHU), Paseo de la Universidad 7, Vitoria 01006, Spain*
[4]*Dipartimento di Chimica, Biologia e Biotecnologie, Università degli Studi di Perugia, Via Elce di Sotto 8, Perugia 06123, Italia*

Accepted XXX. Received YYY; in original form ZZZ

ABSTRACT
We carry out quasi-classical trajectory caculations for the C + $CH^+ \rightarrow C_2^+$ + H reaction on an *ad hoc* computed high-level *ab initio* potential energy surface. Thermal rate coefficients at the temperatures of relevance in cold interstellar clouds are derived and compared with the assumed, temperature-independent estimates publicly available in kinetic databases KIDA and UDfA. For a temperature of 10 K the database value overestimates by a factor of two the one obtained by us (thus improperly enhancing the destruction route of CH^+ in astrochemical kinetic models) which is seen to double in the temperature range 5–300 K with a sharp increase in the first 50 K. The computed values are fitted via the popular Arrhenius–Kooij formula and best-fitting parameters $\alpha = 1.32 \times 10^{-9}$ cm^3s^{-1}, $\beta = 0.10$ and $\gamma = 2.19$ K to be included in the online mentioned databases are provided. Further investigation shows that the temperature dependence of the thermal rate coefficient better conforms to the recently proposed so-called 'deformed Arrhenius' law by Aquilanti and Mundim.

Key words: ISM: molecules – astrochemistry – molecular data – molecular processes

1 INTRODUCTION

The chemical evolution of interstellar clouds can be predicted over time using kinetic models based on estimates of the reaction rates between the hundreds of involved species. In recent years, online repositories such as the KInetic Database for Astrochemistry KIDA (Wakelam et al. 2012) accessible at `http://kida.obs.u-bordeaux1.fr/` or the UMIST (University of Manchester Institute of Science and Technology) Database for Astrochemistry UDfA (Woodall et al. 2007; McElroy et al. 2013) accessible at `http://udfa.ajmarkwick.net/`, have become popular for storing and making publicly available kinetic parameters of thousands of reactions for inclusion in the above mentioned models. Many of the ion-molecule reactions in these databases are modeled by means of simple capture theories whereby the translational energy of reactants must only surpass a long-range centrifugal barrier for reaction to occur. However, the resulting estimates might be inappropriate and as a matter of fact, especially when experimental information is missing, their accuracy has to be assessed against the results of a rigorous, dynamics-based treatment.

Among the simplest and most important processes occurring in the interstellar medium are neutral-ion and neutral-neutral atom-diatom (A + BC) bimolecular reactions involving carbon and hydrogen atoms (Solomon & Klemperer 1972; Herbst 2001). In order to ground the available information on these processes on rigorous theoretical treatments, in the last fifteen years several studies either based on quasi-classical trajectory (QCT) or quantum-reactive-scattering (QRS) techniques have appeared on three-atom systems such as CH_2 (see Bussery-Honvault et al. (2001); Lin et al. (2004); Balucani et al. (2004, 2005); Defazio et al. (2009); Joseph et al. (2011); Sun et al. (2013); Wu et al. (2014) for reaction C + H_2), CH_2^+ (see Herraez-Aguilar et al. (2014) and Zanchet et al. (2013) for reaction C^+ + H_2 and Stoecklin & Halvick (2005); Warmbier & Schneider (2011); Bovino et al. (2015) for reaction CH^+ + H), and C_2H (see Boggio-Pasqua et al. (1998); Tang et al. (2001b,a); Yang et al. (2011) for reaction C + CH). On the contrary, little attention has received the positively charged variant of the latter system, C_2H^+, for which the lowest-energy atom-diatom reaction channel is the exoergic one

$$C\,(^3P_0) + CH^+\,(X^1\Sigma^+) \rightarrow C_2^+\,(X^4\Sigma_g^-) + H\,(^2S_{1/2})\,. \quad (1)$$

Besides being a prototype model for the formation of the carbon-carbon chemical bond, Reaction 1 involves two astrophysically relevant species: the ubiquitous throughout the interstellar space methylidyne cation CH^+ (firstly discovered in the diffuse interstel-

★ To whom correspondence should be addressed. E-mail: srampino@thch.unipg.it

lar medium in 1941 (Douglas & Herzberg 1941)) and the dicarbon cation C_2^+ (detected by the mass-spectroscopic sampling in comets Halley (Krankowsky et al. 1986) and Giacobini-Zinner (Coplan et al. 1987)), which is incorporated in ion-molecule reactions for the production of hydrocarbons in interstellar clouds (Winnewisser 1981).

Presently available estimates for the rate coefficient of Reaction 1 are based on the Langevin capture model (Langevin 1905; Gioumousis & Stevenson 1958; Woon & Herbst 2009; Wakelam et al. 2010). According to this model, the thermal rate coefficient of a reaction involving ion-neutral colliding partners is independent of the temperature and is given by

$$k = 2\pi e \sqrt{\frac{\alpha_D}{\mu}} \tag{2}$$

where e is the charge of the electron, α_D is the dipole polarizability (strictly speaking, the polarizability volume in units of cm^3) of the neutral colliding partner and μ is the reduced mass of the reactants. In 1972, Solomon & Klemperer (1972) estimated for the rate coefficient of Reaction 1 (as well as for most of the ion-neutral astrochemical reactions) a value of 1×10^{-9} cm^3 s^{-1}. A more recent estimate of 1.2×10^{-9} cm^3 s^{-1} was given by Prasad & Huntress (1980) who adopted a dipole-polarizability value for carbon of 1.64×10^{-24} cm^3, which is very near to the most recent theoretical value of 1.67×10^{-24} cm^3 (Thierfelder et al. 2008). The resulting value for the rate coefficient is indeed that one provided by the above mentioned online databases KIDA and UDfA, which make use of the popular Arrhenius–Kooij formula (Kooij 1893) (also known as chemists as modified Arrhenius equation (Laidler 1996))

$$k(T) = \alpha(T/300)^{\beta} e^{-\gamma/T} \tag{3}$$

to express the thermal rate coefficient of bimolecular reactions. In fact, for Reaction 1 both KIDA and UDfA (accessed 2016 April 11) quote $\alpha = 1.2 \times 10^{-9}$ cm^3 s^{-1} and enforce temperature independence by setting $\beta = 0$ and $\gamma = 0$ K. Such estimate is assumed to be valid for a temperature range of 10–280 K in KIDA and 10–41000 K in UDfA (with the claim of an estimated accuracy of a factor of two). In KIDA a second, more recent value of $\alpha = 1.14 \times 10^{-9}$ cm^3 s^{-1} for the same temperature range of 10–280 K is also quoted. This value is worked out from that one already mentioned by taking into account the branching ratios of the $C + CH^+$ reaction to products $C_2^+ + H$ (0.95) and $C_2 + H^+$ (0.05) obtained using a semiempirical model (Chabot et al. 2013) with reactants and products in their electronic ground states. The second channel, however, if reactants and products are taken in their electronic ground state as in Chabot et al. (2013), is endoergic by 0.32 eV. As a consequence, the related reaction is expected not to occur at the temperatures (around 10 K) of the cold, dark, quiescent dense interstellar clouds. We shall therefore hereinafter consider only the former value of $\alpha = 1.2 \times 10^{-9}$ cm^3 s^{-1}.

In this paper we provide accurate thermal rate coefficients for Reaction 1 by computing the potential energy surface (PES) governing the various elementary processes of the system and by integrating the motion equations of the involved nuclei in the Born-Oppenheimer regime. For that purpose, we make use of the grid-empowered molecular simulator GEMS (Laganà 2005; Laganà et al. 2010; Rampino 2011; Rampino et al. 2012) designed to enable the coordinated execution of different codes on distributed platforms by properly selecting compute resources among the high-performance computing (HPC) and high-throughput computing (HTC) available ones on the ground of the quality of the service provided (Manuali et al. 2010; Manuali & Laganà 2014). GEMS is articulated into four highly interoperable (Rampino et al. 2012; Rossi et al. 2014) modules:

(i) INTERACTION: to determine the electronic structure by high-level *ab initio* methods
(ii) FITTING: to build a functional representation of the potential energy values
(iii) DYNAMICS: to carry out dynamics calculations
(iv) OBSERVABLES: to perform the statistical averaging of the dynamical output data to the end of working out an estimate of the observables

and has been successfully used to study the dynamics and compute the reactive probabilities, cross sections and rate coefficients of atom-diatom systems such as $H + H_2$ (Rampino et al. 2012), $Li + FH$ (Laganà & Rampino 2014), $N + N_2$ (Rampino et al. 2009a, 2010b) and $O + O_2$ (Rampino et al. 2009b, 2010a).

Accordingly, we start by illustrating the *ab initio* calculations of the electronic structure of the molecular system leading to Reaction 1 performed using standard procedures on an optimized regular space-reduced bond-order (SRBO) mesh (Rampino 2016) of molecular geometries and fitting the computed potential energy values to the well-known Aguado-Paniagua (AP) functional form (Aguado & Paniagua 1992; Aguado et al. 1998). Then we discuss the outcomes of extended QCT calculations carried out on the resulting analytic, single-sheeted PES to the end of working out the related observables. Computing resources used for running GEMS included the Distributed Computing Infrastructure (DCI) machines of EGI (European Grid Infrastructure, `http://www.egi.eu/`), the IBM PLX supercomputer of Cineca (Italy, `http://www.cineca.it/it/content/ibm-plx`), the Linux Cluster 'Herla' of the INSTM research unit of Perugia (Italy) (Manuali et al. 2014) equipped with NVIDIA GPUs and the machines of the Supercomputing Center for Education & Research of the University of Oklahoma at Norman OK (US, `http://www.oscer.ou.edu/resources.php`).

The paper is organized as follows: In Section 2 the construction of the PES for Reaction 1 is described by making reference to the modules INTERACTION and FITTING. In the same section a graphical inspection is also carried out to the end of singling out possible features of dynamical relevance. In Section 3 the dynamics calculations are described by making reference to the modules DYNAMICS and OBSERVABLES and the temperature dependence of the thermal rate coefficient of Reaction 1 is analyzed. In Section 4 some conclusions and considerations for future work are drawn.

2 INTERACTION AND FITTING

2.1 *Ab initio* calculations

The electronic structure of diatomics CH^+ and C_2^+ was previously investigated in Green et al. (1972); Petrongolo et al. (1981); Kraemer & Roos (1987); Watts & Bartlett (1992); Shi et al. (2013) and the spectroscopic properties of the related ground-states $^1\Sigma^+$ and $^4\Sigma_g^-$, respectively, were determined. C_2H^+ was studied in Krishnan et al. (1981) and Koch & Frenking (1990). Its minimum-energy configuration was found to be collinear ($\widehat{CCH} = 180°$) with electronic ground state $^3\Pi$. Data resulting from the most recent of these calculations are reported in Table 1. In our calculations, that we discuss more extensively in Pacifici et al. (2016), ground-state electronic energies of CH^+, C_2^+ and triplet C_2H^+ were obtained by

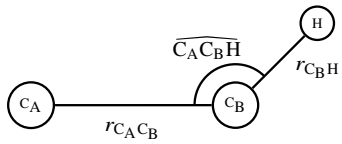

Figure 1. Scheme of the internal coordinates used to describe the reactive channel $C + CH^+ \rightarrow C_2^+ + H$.

second-order multi-reference perturbation theory (MRPT) in the 'partially contracted' PC-NEVPT2 approach (Angeli et al. 2002, 2007) using complete-active-space self-consistent-field (CASSCF) reference wavefunctions as implemented in the MOLPRO package version 2010.1 (Werner et al. 2010). Following the work on the ground- and excited-state potential energy curves of the C_2 molecule by Angeli et al. (2012), we adopt here the atomic-natural-orbital relativistic-correlation-consistent (ANO-RCC) basis set (Widmark et al. 1990; Roos et al. 2004) and the Douglas-Kroll-Hess Hamiltonian (Hess 1986) to properly account for scalar relativistic effects. The full $2s$ and $2p$ valence space was used to define the CASSCF wavefunctions. Results on the equilibrium properties of the considered diatoms and triatom are reported in Table 1 and show to agree with previous calculations and available experimental data. According to the computed *ab initio* values, Reaction 1 is exoergic by 1.65 eV.

To the purpose of building a functional representation of the PES for Reaction 1, a set of *ab initio* energies at several relevant molecular geometries have to be computed. Configuration-space sampling (i.e., the choice of these geometries) was accomplished according to the space-reduced bond-order (SRBO) grid approach of Rampino (2016). In the SRBO scheme, use is made of opportunely defined diatomic bond-order (BO) variables (Garcia & Laganà 1985a,b)

$$n = e^{-\beta_{BO}(r-r_e)} \tag{4}$$

with r being the diatom internuclear distance and r_e its equilibrium value. SRBO variables are obtained by fixing two boundary r_{min} and r_{max} values and relaxing β_{BO} so as to reach a desired ratio f between the sampled attractive ($e^{-\beta_{BO}(r_{max}-r_e)} < n < 1$) and repulsive ($1 < n < e^{-\beta_{BO}(r_{min}-r_e)}$) regions of the diatom configuration space (see also Rampino & Laganà 2012). Reasonable boundary values can be obtained via a Morse modeling of the diatom potential through parameters V_{fact} and V_{thrs} (set here to 1.0 and 0.01, respectively) for which the reader is referred to Rampino (2016). The diatom configuration space is then conveniently sampled by a uniform grid in BO variables which is denoted by (N_r, N_a) with N_r and N_a being the number of points in the repulsive and attractive regions, respectively, resulting in a space ratio parameter $f = N_a/N_r$. The associated SRBO grid consists of $N_r + N_a + 1$ total number of points, the added one accounting for the equilibrium geometry which is neither attractive nor repulsive.

For the two two-body CH^+ and C_2^+ terms of the potential, *ab initio* energies were computed on a 10-point (3, 6) SRBO grid in coordinates r_{CH} and r_{CC}, respectively (see a scheme in Fig. 1 of the coordinates used to model the reactive channel under study). As to the three-body term, though focus in this paper is on reaction channel $C_A + C_BH^+ \rightarrow C_AC_B^+ + H$ (where subscripts A and B have been used to distinguish the two carbon atoms) we also accounted for the alternative one $C_A + HC_B^+ \rightarrow C_AH^+ + C_B$. To model the first of these two channels, use was made of the above defined SRBO grids for r_{C_BH} and $r_{C_AC_B}$ plus an angular grid for $\widehat{C_AC_BH}$ ranging from 180° to 60° in steps of 30° (for a total of $10 \times 10 \times 5 = 500$ points). To model the second channel, use was made of analogous SRBO grids for r_{HC_B} and r_{C_AH} plus an angular grid for $\widehat{C_AHC_B}$ ranging from 180° to 60° in steps of 30° (for a total number of points of $\frac{10\times(10+1)}{2} \times 5 = 275$ because of the symmetry specific to this channel).

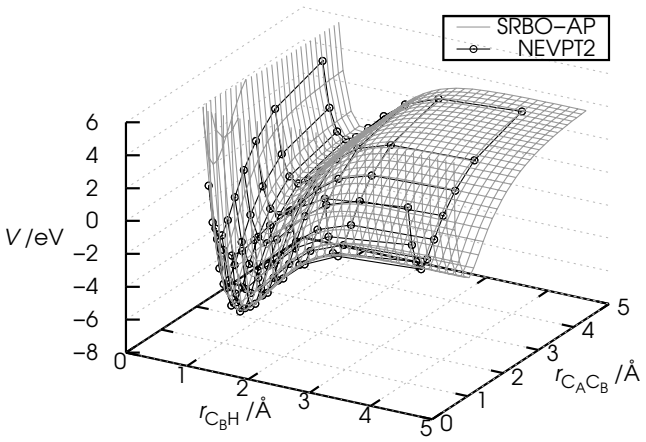

Figure 2. Two-dimensional representation of the PES for the $C + CH^+ \rightarrow C_2^+ + H$ reactive channel at fixed angle $\widehat{C_AC_BH} = 120°$. Black circles/black mesh: computed *ab initio* energies. Gray mesh: fitted PES. The energy zero is set to the bottom of the reactant valley.

2.2 Potential energy surface

The final PES including both reactive channels was built via an AP global fit to the resulting three-body set of 775 points plus the two two-body sets of 10 points each. The AP fit was carried out using the GFIT3C program (Aguado et al. 1998) employing a 6th-degree polynomial fit for the two-body terms and a 7th-degree polynomial fit for the three-body term. For illustrative purposes we show in Fig. 2 the set of calculated *ab initio* points (black circles and mesh) at fixed angle $\widehat{C_AC_BH} = 120°$ and the fitted PES (gray mesh) for the $C + CH^+ \rightarrow C_2^+ + H$ reactive channel. As apparent from the figure, the distribution of the computed *ab initio* points indicates a fair coverage of the molecular geometry space by the SRBO grid used for the calculations, with a denser concentration in the high-gradient regions of the potential. The figure also shows the smoothness of the fitted PES and the occurrence of a deep well in the strong interaction region.

The equilibrium properties of the diatomic and triatomic fragments as resulting from the fitted PES (SRBO-AP) are given in Table 1. As apparent from the table, the fitted PES reproduces fairly well the data resulting from the present *ab initio* calculations and those from previous theoretical and experimental works, providing an exoergicity for Reaction 1 of 1.64 eV.

Isoenergetic contours of the collinear ($\widehat{C_AC_BH} = 180°$) channel for Reaction 1 are shown in Fig. 3 in order to support the analysis of the structural properties of the reactive process. In the figure, the entry channel for Reaction 1 is located in the bottom right area of the plot (low values of the reactant-diatom bond length r_{C_BH}, high values of the distance between the colliding carbon and the bound one $r_{C_AC_B}$). The collinear reaction proceeds barrierless towards a deep well (more than 6.7 eV from the bottom of the reactant channel) in the strong interaction region at short distances in the bottom left area of the plot. The exoergic product channel is reached in the top left area of the plot. The long-range regions of the fitted PES connect

Table 1. Equilibrium distances r_e and dissociation energies D_e of CH^+, C_2^+ and C_2H^+ as resulting from the fitted SRBO-AP PES, from the present *ab initio* calculations (NEVPT2), and from previous theoretical (Calc.) and experimental (Expt.) works.

CH^+ ($X^1\Sigma^+$)

	r_e /Å	D_e /eV
SRBO-AP	1.13	4.08
NEVPT2	1.13	4.08
Calc. (Green et al. 1972)	1.13	4.11
Expt. (Huber & Herzberg 1979)	1.13	4.25

C_2^+ ($X^4\Sigma_g^-$)

	r_e /Å	D_e /eV
SRBO-AP	1.42	5.72
NEVPT2	1.41	5.73
Calc. (Shi et al. 2013)	1.41	5.71
Expt. (Maier & Rösslein 1988)	1.40	
Expt. (Huber & Herzberg 1979)	1.30	5.4

C_2H^+ ($X^3\Pi$, $\widehat{C_AC_BH} = 180°$)

	r_e^{CC} /Å	r_e^{CH} /Å	D_e /eV
SRBO-AP	1.28	1.08	10.79
NEVPT2	1.26	1.08	10.94
Calc. (Koch & Frenking 1990)	1.27	1.09	

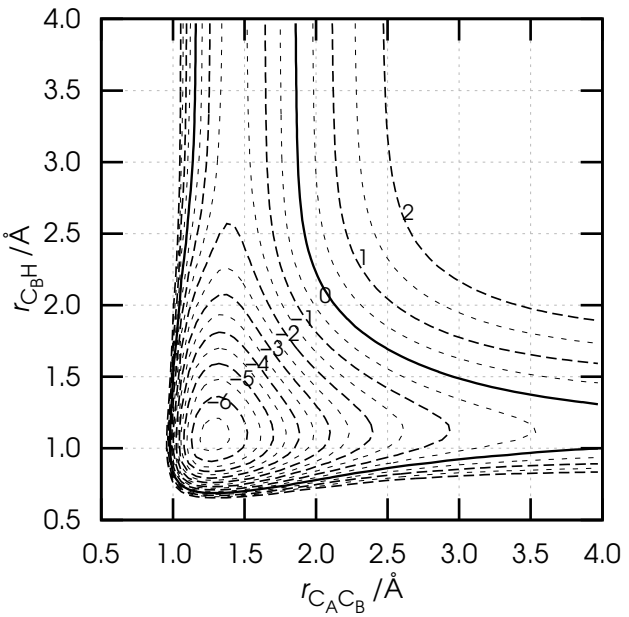

Figure 3. Isoenergetic contours (from −6.5 to 2 eV in steps of 0.5 eV) of the SRBO-AP PES for the collinear reaction channel $C + CH^+ \rightarrow C_2^+ + H$. Energy zero set to the bottom of the reactant valley.

smoothly to the short-range without exhibiting spurious structures. Contours for bent approaches show a similar behavior though with a decreasing well depth reaching −5.6 eV at $\widehat{C_AC_BH} = 60°$.

3 DYNAMICS AND OBSERVABLES

3.1 Details of dynamical computations

A rigorous treatment of molecular reactive collisions should include quantum effects. However, the huge number of vibro-rotational states involved (mainly for the C_2^+ product molecule) prevents the use of quantum dynamical methodologies. Therefore, the quasi-classical trajectory method (Karplus et al. 1965) becomes the most appropriate technique to study Reaction 1. The term 'quasi-classical' denotes that the molecules are selected before the collision at discrete internal energy states corresponding to quantum states. After the collision, a 'quantization' of the internal energy is also enforced on the product molecule. In this work, QCT calculations were carried out using the program VENUS96 (Hase et al. 1996).

The QCT method assumes that the nuclei involved in a chemical reaction move according to the laws of classical mechanics on the potential energy surface of the system. By integrating the Hamilton equations the coordinates and momenta of all nuclei are calculated at any time during the collision. The integration is carried out until the fragments produced by the collision are sufficiently separated. Then, the species produced are identified and the channel (non reactive, reactive or dissociative) is assigned. The result of the integration is a set of final values for coordinates and momenta of all the nuclei. By using this information, final properties of the system (like, for instance, the internal energies and rotational angular momenta of the molecules, the (approximate and continuous) rotational and vibrational 'quantum numbers' of molecules, the relative translational energy, the scattering angle) are evaluated.

However, the outcome of a single trajectory is insufficient to describe the reaction characteristics. To this end, a statistically significant sample of trajectories has to be integrated and related outcomes averaged. In the QCT framework, the reaction cross section is estimated by:

$$\sigma = \pi b_{max}^2 \frac{N_r}{N}$$

where N is the total number of trajectories integrated, N_r the number of reactive trajectories and b_{max} is the maximum value of the impact parameter leading to reaction. The error in this estimation is proportional to $N_r^{-1/2}$.

Similarly, an estimate of the thermal rate coefficient is given by the product of the reaction cross section and the average velocity $\langle v \rangle$ at the temperature T (Truhlar & Muckerman 1979):

$$k(T) = \sigma \langle v \rangle = \left(\frac{8 k_B T}{\pi \mu} \right)^{1/2} \pi b_{max}^2 \frac{N_r}{N}$$

where k_B and μ represent the Boltzmann's constant and the reduced mass of the reactants respectively.

Three blocks of calculations were carried out to determine separately thermal rate coefficients, state-specific rate coefficients, and cross sections.

The first block was aimed at calculating the fully thermal rate coefficient, $k(T)$. To this purpose, the collision energies were selected according to the Boltzmann distribution at temperature T. The initial vibro-rotational states were selected also following a Boltzmann distribution for temperature T over the manifold of states supported by the diatomic potential curve. Thermal rate coefficients were calculated at 56 temperatures in the range from 5 K to 300 K, with a finer sampling for lower temperatures (steps of 1 K in the range 5–20 K, 2 K in the range 22–48 K and 10 K in the range 50–300 K). A total of $N = 4 \times 10^6$ trajectories were integrated for each

considered temperature, leading to an error on the rate coefficient lower than 1%.

The second block was aimed at calculating the state-specific rate coefficients. In this case, the collision energies were also selected according to the Boltzmann distribution at temperature T while a single initial vibro-rotational state was set. State-specific rate coefficients where calculated starting from both the ground and the first excited vibrational state ($v = 0$ and $v = 1$) and from both the ground and the first excited rotational state ($j = 0$ and $j = 1$). The vibro-rotational energies of the diatomic molecules were computed by semiclassical quantization of the action using the asymptotes of the potential energy surface as potential energy curves (Truhlar & Muckerman 1979). The same temperatures and number of trajectories used for the calculation of the thermal rates coefficients were considered in this second block.

The third block of calculations was aimed at calculating state-specific cross sections. The same states ($v = 0, j = 0$), ($v = 0, j = 1$), ($v = 1, j = 0$) and ($v = 1, j = 1$) were considered. Cross sections were calculated for the mentioned vibro-rotational states in a collision-energy range from 4.33×10^{-5} to 0.03 eV. In this case, $N = 2 \times 10^6$ trajectories were integrated for each collision energy leading to an error on the reaction cross section lower than 0.5%.

Some details on the selection of parameters for the trajectory integration follow. As known, the interaction between an ion and a neutral particle extends to large distances. For this reason, initial and final distances to start and to end the trajectory integration were set at 25.0 Å. At this distance the interaction between the fragments of the related channels is smaller than 3×10^{-7} eV. Analogously, the maximum impact parameter was set at 20.0 Å in order to ensure that all reactive collisions are taken into account. The integration step was set at 0.05 fs. This value guarantees a total energy conservation better than 2×10^{-7} eV, even at the lowest considered temperature.

For the sake of comparison, we checked our QCT results against exact quantum calculations in the energy interval 4.33×10^{-5}–0.03 eV getting a deviation of less than 10% from the quantum average value. The reader is referred to the already quoted Pacifici et al. (2016) for a more detailed discussion.

3.2 Computed observables

The computed thermal and state-specific rate coefficients are shown in Fig. 4 as a function of the temperature T. The Langevin-model KIDA and UDfA value is also represented (horizontal dot-dashed line). As the figure shows, the computed thermal rate coefficient increases more than a factor of two (from 0.6×10^{-9} to 1.3×10^{-9} $cm^3\ s^{-1}$) in going from $T = 5$ K to $T = 300$ K with a pronounced increase up to 50 K. The thermal rate coefficient at 10 K is 0.7×10^{-9} $cm^3\ s^{-1}$, about one half of the assumed value in the KIDA and UDfA databases. As apparent from the figure, the largest contribution to the value of the thermal rate coefficient is that associated with the ground ($v = 0$, $j = 0$) vibro-rotational state. The figure also shows that an increase of the excitation of either the vibration or the rotation of the reactants lowers the value of the rate coefficient.

In order to better understand the microscopic origin of such effect we calculated also state-specific reactive cross sections $\sigma_{v,j}(E_{tr})$ which are shown in Figure 5 for a collision-energy (E_{tr}) interval 4.33×10^{-5}–0.03 eV. As apparent from the figure, cross sections for the different vibro-rotational blocks tend to decrease and converge as translational energy increases while they tend to increase and diverge as translational energy decreases. This confirms that, as expected for a barrierless reactive process, the key

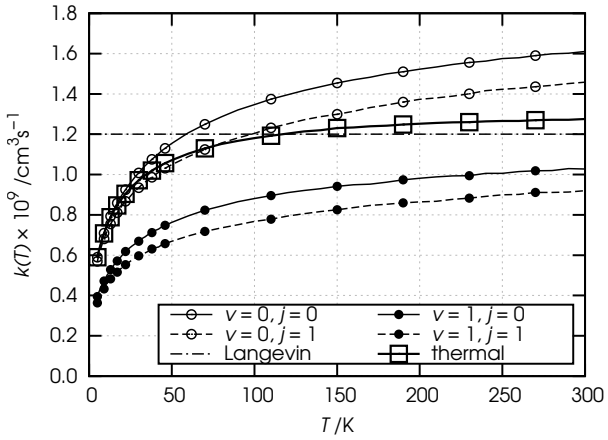

Figure 4. Thermal and state-specific rate coefficient for the reactive process C + CH^+ $(v, j) \rightarrow C_2^+$ + H plotted as a function of the temperature T. The temperature-independent capture-model values is also reported (dot-dashed line).

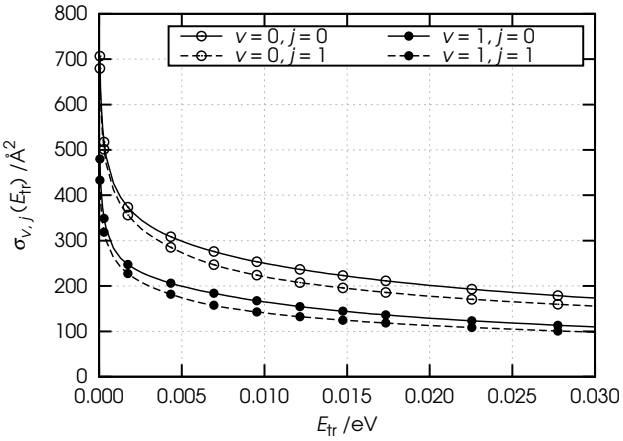

Figure 5. State-specific cross sections for reaction C + CH^+ $(v, j) \rightarrow C_2^+$ + H plotted as a function of the translational energy E_{tr}.

driving factor to reaction is the gradient of the PES while an increase of collision and internal energies reduces reactivity by acting as antagonist factors.

These findings prompted us to a more detailed analysis of the possible paths leading to Reaction 1 on the fitted PES. A representation of the features of the PES useful for rationalizing the outcomes of dynamics calculations is given in Fig. 6 that shows the minimum energy path (MEP) plotted as a function of the reaction coordinate η (i.e., the potential energy at each η value minimized with respect to all remaining coordinates) defined as $\eta = \tan^{-1}(r_{C_BH}/r_{C_AC_B})$. Both the absolute MEP (solid line) and the collinearly ($\widehat{C_AC_BH} = 180°$)-restrained one (dot-dashed line) are shown.

As apparent from Fig. 6, the most favorable path to reaction is the collinear one, with C approaching CH^+ from the carbon side and leading to formation of the linear C_2H^+ intermediate (first well at η about 40°). The collinear path remains the favorable one up to a value of η of about 50°, where the absolute minimum-energy path to products distorts from collinearity and branches symmetrically to a second well either at $\widehat{C_AC_BH} = 0°$ or 360°. This corresponds

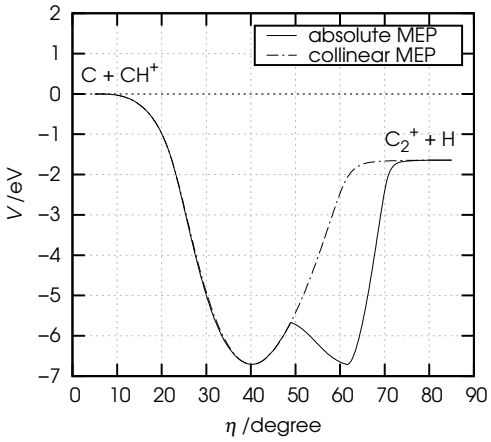

Figure 6. Absolute (solid line) and collinear (dot-dashed line) minimum-energy path (MEP) for the reactive processes $C + CH^+ \rightarrow C_2^+ + H$ plotted as a function of the reaction coordinate η. The energy zero is set to the bottom of the reactant valley.

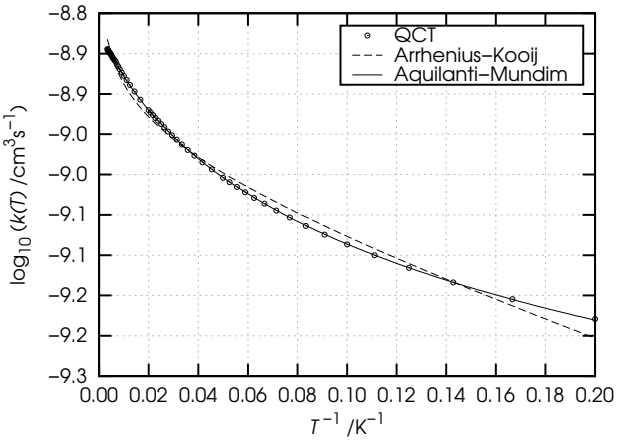

Figure 7. Arrhenius plot of the QCT thermal rate coefficient (solid circles) and of the Arrhenius–Kooij (dashed line) and Aquilanti–Mundim (solid line) best-fitting curves.

to the symmetric rotation of the H atom about the carbon-carbon diatom leading, after the overcoming of a small barrier (1.04 eV), to a structurally identical intermediate with the H atom binding the C colliding atom (second well at η about 60°).

This feature of the PES rationalizes why the cross section decreases not only with translational energy but also with a vibrational and rotational excitation. In fact, an increase of the internal energy has the effect of deviating the system from following the straightforward collinear MEP driven reactive dynamics.

3.3 A parametrized formulation of the computed rate coefficients

The clear temperature dependence of the calculated values of the thermal rate coefficient (shown in Fig. 7 as solid circles in an Arrhenius plot) motivated us to determine the related best-fitting parameters of Eq. 3. The obtained values of α, β and γ are given in Table 2 where also χ^2 and correlation-coefficient values are reported. As apparent from Fig. 7, the Arrhenius–Kooij best-fitting curve (dashed line) is essentially good but shows positive deviations in the central part and negative ones at the external sides, which are more evident at the lowest considered temperatures.

A more flexible parametrized formulation of the temperature dependence of the rate coefficient that was recently proposed by Aquilanti and Mundim is the so-called 'deformed Arrhenius' one (Aquilanti et al. 2010, 2012)

$$k(T) = A\left[1 - d\frac{\epsilon}{RT}\right]^{\frac{1}{d}} \quad (5)$$

where R is the gas constant and A, d and ϵ/R parameters to be determined (Silva et al. 2013; Cavalli et al. 2014; Coutinho et al. 2015). For a comparison, we repeated the non-linear fit using the Aquilanti–Mundim formula. The resulting best-fitting parameters A, d and ϵ/R are given in Table 2. The Aquilanti–Mundim best-fitting curve is shown as solid line in Fig. 7, where deviations from the calculated rate-coefficient values are barely perceivable. The better suitability of the Aquilanti–Mundim law with respect to the conventional Arrhenius–Kooij formulation is further confirmed by the χ^2 and correlation-coefficient (very close to unity) values reported in Table 2.

Table 2. Results of the non-linear fit of the Arrhenius–Kooij and Aquilanti–Mundim equations to the computed QCT thermal rate coefficients.

Arrhenius–Kooij (Eq. 3)

α /cm^{3}s^{-1}	β	γ /K	χ^2	corr. coeff.
1.32×10^{-9}	0.10	2.19	0.0190	0.99628

Aquilanti–Mundim (Eq. 5)

A /cm^{3}s^{-1}	d	(ϵ/R) /K	χ^2	corr. coeff.
1.34×10^{-9}	− 2.73	15.61	0.0001	0.99997

4 CONCLUSIONS AND FUTURE DEVELOPMENTS

In this paper we apply an accurate dynamical treatment to the calculation of the rate coefficients of formation of C_2^+ from CH^+ in collisions with C by following the consolidated workflow scheme of GEMS. In this way, after performing high-level *ab initio* calculations on an SRBO grid of molecular geometries, fitting the calculated values using a well established fitting procedure and performing QCT dynamical calculations of the rate coefficient it was found that such quantity increases of more than a factor of two when the temperature raises from 5 to 300 K.

A comparison of our results with those of model calculations that are widely employed in astrochemical networks, unveils that the latter cannot deal with the temperature dependence singled out by an accurate dynamical treament. At a temperature of 10 K the so far assumed, temperature-independent value in databases KIDA and UDfA overestimates by a factor of about two that one computed by us, thus improperly enhancing the destruction route of CH^+ in astrochemical kinetic models. Moreover, it was also found that the popular Arrhenius–Kooij formulation of the rate coefficient (for which best-fitting parameters α, β and γ to be included in KIDA and UDfA were provided) adopted for this type of reactions might not be accurate enough to give an acceptable fit in the investigated range, a better fit being provided by the recently proposed Aquilanti–Mundim formulation.

The most important consideration, however, is the one concerned with the type of averaging made when evaluating observable properties of reactive systems out of the computed probabilities (either on the impact parameter only (for the cross section) or on

both the impact parameter and the energy distribution (for the rate coefficient)). As discussed in the paper, in fact, the sensitivity of such properties to the parameters controlling the reactive process varies dramatically and might impact significantly the formulation of the quantities to be stored in the related databases.

A further consideration on the use of the reported calculations is the fact that for small molecules it is possible to compare QCT outcomes with QRS ones (especially again within the GEMS workflow) and this is what we are already running in our Laboratories.

ACKNOWLEDGEMENTS

Financial support is acknowledged from the Phys4entry FP7/2007-2013 project (Contract 242311) and the EGI-Inspire project (Contract 261323). Financial support from the Spanish Ministry of Science and Innovation (grant CTQ2012-37404) is also acknowledged. The European Grid Infrastructure (EGI) through the COMPCHEM Virtual Organization, the Italian CINECA computing centre and the OU Supercomputing Center for Education & Research (OSCER) at the University of Oklahoma (OU) are acknowledged for providing computing resources and services. EG and LP thank the European COST Action CM1401 'Our Astro-chemical History' for the funding of short-term scientific missions. The authors are grateful to Prof. Nadia Balucani for stimulating and helpful discussion.

REFERENCES

Aguado A., Paniagua M., 1992, J. Chem. Phys., 96, 1265
Aguado A., Tablero C., Paniagua M., 1998, Comput. Phys. Commun., 108, 259
Angeli C., Cimiraglia R., Malrieu J.-P., 2002, J. Chem. Phys., 117, 9138
Angeli C., Pastore M., Cimiraglia R., 2007, Theor. Chem. Acc., 117, 743
Angeli C., Cimiraglia R., Pastore M., 2012, Mol. Phys., 110, 2963
Aquilanti V., Mundim K. C., Elango M., Kleijn S., Kasai T., 2010, Chem. Phys. Lett., 498, 209
Aquilanti V., Mundim K. C., Cavalli S., De Fazio D., Aguilar A., Lucas J. M., 2012, Chem. Phys., 398, 186
Balucani N., et al., 2004, Phys. Chem. Chem. Phys., 6, 4957
Balucani N., et al., 2005, J. Chem. Phys., 122, 234309
Boggio-Pasqua M., Halvick P., Rayez M.-T., J.-C. R., Robbe J.-M., 1998, J. Phys. Chem. A, 102, 2009
Bovino S., Grassi T., Gianturco F. A., 2015, J. Phys. Chem. A
Bussery-Honvault B., Honvault P., Launay J.-M., 2001, J. Chem. Phys., 115, 10701
Cavalli S., Aquilanti V., Mundim K. C., De Fazio D., 2014, J. Phys. Chem. A, 118, 6632
Chabot M., Béroff K., Gratier P., Jallat A., Wakelam V., 2013, ApJ, 771, 90
Coplan M. A., Ogilvie K. W., A'Hearn M. F., Bochsler P., Geiss J., 1987, J. Geophys. Res.: Space Phys., 92, 39
Coutinho N. D., Silva V. H. C., de Oliveira H. C. B., Camargo A. J., Mundim K. C., Aquilanti V., 2015, J. Phys. Chem. Lett., 6, 1553
Defazio P., Petrongolo C., Bussery-Honvault B., Honvault P., 2009, J. Chem. Phys., 131, 114303
Douglas A. E., Herzberg G., 1941, ApJ, 94, 381
Garcia E., Laganà A., 1985a, Mol. Phys., 56, 621
Garcia E., Laganà A., 1985b, Mol. Phys., 56, 629
Gioumousis G., Stevenson D. P., 1958, J. Chem. Phys., 29, 294
Green S., Bagus P. S., Liu B., McLean A. D., Yoshimine M., 1972, Phys. Rev. A, 5, 1614
Hase W. L., et al., 1996, Quantum Chemistry Program Exchange Bulletin, 16, 43
Herbst E., 2001, Chem. Soc. Rev., 30, 168
Herraez-Aguilar D., Jambrina P. G., Menendez M., Aldegunde J., Warmbier R., Aoiz F. J., 2014, Phys. Chem. Chem. Phys., 16, 24800
Hess B. A., 1986, Phys. Rev. A, 33, 3742
Huber K., Herzberg G., 1979, Molecular Spectra and Molecular Structure. IV Constants of diatomic molecules. Springer US, doi:10.1007/978-1-4757-0961-2_2
Joseph S., Caridade P. J. S. B., Varandas A. J. C., 2011, J. Phys. Chem. A, 115, 7882
Karplus M., Porter R. N., Sharma R. D., 1965, J. Chem. Phys., 43, 3259
Koch W., Frenking G., 1990, J. Chem. Phys., 93, 8021
Kooij D. M., 1893, Z. Phys. Chem., Abt. B, 12, 155
Kraemer W. P., Roos B., 1987, Chem. Phys., 118, 345
Krankowsky D., et al., 1986, Nature, 321, 326
Krishnan R., Frisch M. J., Whiteside R. A., Pople J. A., Schleyer P. v. R., 1981, J. Chem. Phys., 74, 4213
Laganà A., 2005, in Laganà A., Lendvay G., eds, NATO Science Series II: Mathematics, Physics and Chemistry, Vol. 145, Theory of Chemical Reaction Dynamics. Springer Netherlands, pp 363–380, doi:10.1007/1-4020-2165-8_17
Laganà A., Rampino S., 2014, Lect. Notes Comput. Sci., 8579, 571
Laganà A., Costantini A., Gervasi O., Faginas Lago N., Manuali C., Rampino S., 2010, J. Grid Comput., 8, 571
Laidler K., 1996, Pure Appl. Chem., 68, 149
Langevin P., 1905, Ann. Chim. Phys., 5, 245
Lin S. Y., Guo H., 2004, J. Phys. Chem. A, 108, 10066
Maier J. P., Rösslein M., 1988, J. Chem. Phys., 88, 4614
Manuali C., Laganà A., 2014, VIRT&L-COMM, 5, 5
Manuali C., Laganà A., Rampino S., 2010, Comput. Phys. Commun., 181, 1179
Manuali C., Costantini A., Vitillaro G., Laganà A., 2014, VIRT&L-COMM, 5, 5
McElroy D., Walsh C., Markwick A. J., Cordiner M. A., Smith K., Millar T. J., 2013, A&A, 550
Pacifici L., Pastore M., Garcia E., Laganà A., Rampino S., 2016, J. Phys. Chem. A, doi: 10.1021/acs.jpca.6b00564
Petrongolo C., Bruna P. J., Peyerimhoff S. D., Buenker R. J., 1981, J. Chem. Phys., 74, 4594
Prasad S. S., Huntress Jr. W. T., 1980, ApJ, 239, 151
Rampino S., 2011, PhD thesis, Università degli Studi di Perugia
Rampino S., 2016, J. Phys. Chem. A, doi: 10.1021/acs.jpca.5b10018
Rampino S., Laganà A., 2012, Int. J. Quantum. Chem., 112, 1818
Rampino S., Skouteris D., Laganà A., García E., Saracibar A., 2009a, Phys. Chem. Chem. Phys., 11, 1752
Rampino S., Skouteris D., Laganà A., 2009b, Theor. Chem. Acc., 123, 249
Rampino S., Skouteris D., Laganà A., 2010a, Int. J. Quantum. Chem., 110, 358
Rampino S., Garcia E., Pirani F., Laganà A., 2010b, Lect. Notes Comput. Sci., 6019, 1
Rampino S., Monari A., Rossi E., Evangelisti S., Laganà A., 2012, Chem. Phys., 398, 192
Roos B. O., Lindh R., Malmqvist P.-Å., Veryazov V., Widmark P.-O., 2004, J. Phys. Chem. A, 108, 2851
Rossi E., et al., 2014, J. Comput. Chem., 35, 611
Shi D., Niu X., Sun J., Zhu Z., 2013, J. Phys. Chem. A, 117, 2020
Silva V. H. C., Aquilanti V., de Oliveira H. C., Mundim K. C., 2013, Chem. Phys. Lett., 590, 201
Solomon P. M., Klemperer W., 1972, ApJ, 178, 389
Stoecklin T., Halvick P., 2005, Phys. Chem. Chem. Phys., 7, 2446
Sun Z. S., Zhang C., Lin S., Zheng Y., Meng Q., Bian W. B., 2013, J. Chem. Phys., 139, 014306
Tang B.-Y., Chen M.-D., Han K.-L., Zhang J. Z. H., 2001a, J. Phys. Chem. A, 105, 8629
Tang B.-Y., Chen M.-D., Han K.-L., Zhang J. Z. H., 2001b, J. Chem. Phys., 115, 731
Thierfelder C., Assadollahzadeh B., Schwerdtfeger P., Schäfer S., Schäfer R., 2008, Phys. Rev. A, 78, 052506, see also `http://ctcp.massey.ac.nz/Tablepol2014.pdf` (accessed 2016 April 11)
Truhlar D. G., Muckerman J. T., 1979, in Bernstein R. B., ed., , in Atom-Molecule Collision Theory. Springer US, pp 505–566, doi:10.1007/978-1-4613-2913-8_16

Wakelam V., et al., 2010, Space Sci. Rev., 156, 13
Wakelam V., et al., 2012, ApJS, 199, 21
Warmbier R., Schneider R., 2011, Phys. Chem. Chem. Phys., 13, 10285
Watts J. D., Bartlett R. J., 1992, J. Chem. Phys., 96, 6073
Werner H.-J., et al., 2010, MOLPRO, version 2010.1, a package of ab initio programs, see http://www.molpro.net (accessed 2016 April 11)
Widmark P.-O., Malmqvist P.-Å., Roos B., 1990, Theor. Chim. Acta, 77, 291
Winnewisser G., 1981, Top. Curr. Chem., 99, 39
Woodall J., Agundez M., Markwick-Kemper A. J., Millar T. J., 2007, A&A, 466, 1197
Woon D. E., Herbst E., 2009, ApJS, 185, 273
Wu Y., Zhang C., Cao J., Bian W., 2014, J. Phys. Chem. A, 118, 4235
Yang H., Hankel M., Zheng Y., Varandas A. J. C., 2011, J. Chem. Phys., 135, 024306
Zanchet A., Godard G., Bulut N., Roncero O., Halvick P., José C., 2013, ApJ, 766, 80

This paper has been typeset from a TEX/LATEX file prepared by the author.